Contr. Mineral. and Petrol. 27, 131—158 (1970)

Chemical Composition and Physical Properties of Lithium-Iron Micas from the Krušné hory Mts. (Erzgebirge)

Part A; Chemical Composition

Milan Rieder

Department of Earth and Planetary Sciences, Johns Hopkins University, Baltimore, Maryland, U.S.A.*

Chemical Analyses by

Miroslav Huka**, Dagmar Kučerová**, Luděk Minařík***, Jiří Obermajer**, and Pavel Povondra***

Abstract. Compositions of natural lithium-iron micas are approximated best by the siderophyllite-polylithionite join. These micas contain little or no magnesium and manganese. Their octahedral sheets contain close to two trivalent cations (mainly aluminum) in small crystallographic sites and a variable quantity of lithium and R^{+2} (mainly iron) in large sites. Octahedral vacancies are situated mostly in large sites. Lithium and R^{+2} approach a 4:4 replacement relationship in micas with octahedral occupancy close to six. Lithium and fluorine show a good positive correlation (small excess of fluorine over lithium), which indicates a crystallochemical association between them. There is a less distinct positive correlation between lithium and R^{+4}.

Based on simplifications, a calculation shows that about two-thirds of octahedral vacancies are caused by substitutions within the octahedral sheet, one-third, by tetrahedral substitutions. Different methods of calculating the crystallochemical formula yield slightly different numbers of octahedral vacancies, but do not affect the mica's position in plots of physical parameters against composition. If a crystallochemical formula is calculated from analysis of a mica contaminated with quartz, topaz, or feldspar, the apparent number of octahedral vacancies increases; such a formula exhibits unusual behavior in composition plots.

1. Introduction

Lithium-iron micas are a typical constituent of greisens, some granites and pegmatites, and fillings of hydrothermal veins of the tin-tungsten-molybdenum formation (Cissarz, 1927). These rocks and veins are important as the source of tin, tungsten, molybdenum, and lithium. It is now agreed that greisens formed by epigenetic alteration of granitic rocks and their mantle. Opinions differ on individual aspects of the process, its continuity or discontinuity in particular (Štemprok, 1965, 1967). A general prospection-oriented study of greisens and associated veins in the Krušné hory Mts. (Erzgebirge) was sponsored by the Ústřední ústav geologický in Praha. The study of lithium-iron micas was initiated as a part of this project.

The greisens have a characteristic mineralogy: quartz-mica-fluorite-topaz $\pm$ feldspar. Among these minerals, mica is the only chemically complex phase; the

* Present address: Ústav geologických věd University Karlovy (Institute of Geological Sciences, Charles University), Albertov 6, Praha 2, Czechoslovakia.

** Ústřední ústav geologický (Geological Survey of Czechoslovakia), Praha, Czechoslovakia.

*** Československá akademie věd (Czechoslovak Academy of Sciences), Praha, Czechoslovakia.

knowledge of its geochemical history might enhance our understanding of the origin of these rocks.

Specimens of micas from greisens and associated veins were collected and chemically analyzed. Concomitantly, single-crystal X-ray and optical study was performed. Physical parameters were correlated with chemical composition. Based on the knowledge of compositions and crystallography of natural lithium-iron micas, synthetic micas were grown and studied at elevated pressures and temperatures as a first step in experimental modelling of the greisens.

This paper deals with chemical composition of natural lithium-iron micas. Their cell parameters and optical properties will appear as Part B. Results of the study of polytypism, twinning, and epitaxy will be published elsewhere; so will be the results of experimental work on synthetic lithium-iron micas.

2. Chemical Analyses

2.1. Material for Analysis

Tin-tungsten deposits of the Krušné hory Mts. (Erzgebirge) in Czechoslovakia and German Democratic Republic have been exploited for several centuries. The geology of these deposits, such as Cínovec, Krupka, Slavkov[1], or Altenberg (Fig. 1), is well known. They yield a number of lithium-iron micas, which were selected for study. Four non-greisen micas were included: a biotite from the Budeč skarn and three lepidolites from pegmatites at Radkovice and Biskupice (all Czechoslovakia).

Micas from greisens and associated veins used to be referred to as zinnwaldite, protolithionite, Li-biotite, or cryophyllite (Table 1, discussion of nomenclature in chapter 3). The micas are associated with quartz, topaz, fluorite, albite, cassiterite, wolframite, and molybdenite.

The iron-rich micas are black or green-black; zinnwaldite is light greyish green to light amber; the color of lithium-rich varieties is light purple. Upon weathering the micas turn brownish or brown, as bivalent iron is oxidized. Changes of the F:OH ratio of the micas also affect the color. Most micas are hypautomorphic, only a few specimens contained automorphic crystals in cavities. Twinning can be observed megascopically, especially in coarse-grained zinnwaldite. Grain size varies from less than one millimeter in micas from fine-grained greisens to several centimeters in micas from veins, pegmatites, or the so-called *Stockscheider*.

Of the thirty micas analyzed, six come from mines, six from drilling cores, and eighteen from surface works. Only unweathered micas were collected. Heterogeneous impurities were separated by hand under a binocular microscope. Fine-grained micas were further purified by magnetic and heavy-liquid methods. Despite this, small amounts of P_2O_5 and S^{-2} were detected by the analysis and subtracted as apatite and pyrite. Besides, the analyses average out compositional variation within individual samples, such as fine zoning of crystals. For example, two separate Li_2O determinations in one zinnwaldite book yielded 4.66 and 4.25% (Štemprok, 1961).

1 Known also under German names Zinnwald, Graupen, Schlaggenwald, respectively.

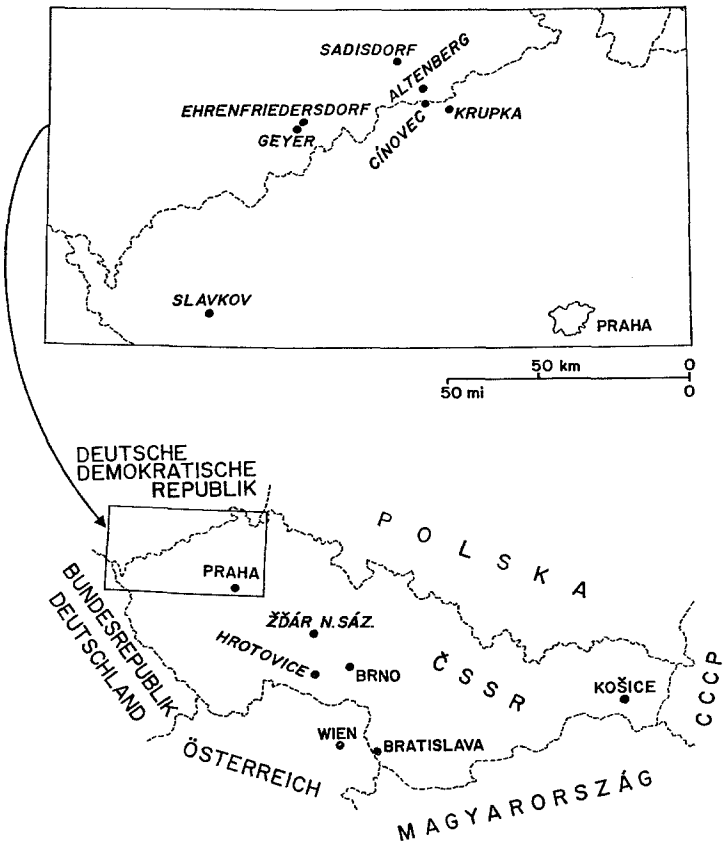

Fig. 1. Localities of lithium-iron micas studied (slanted lettering)

2.2. Calculation of Crystallochemical Formula

The micas were chemically analyzed in 1965—1967. The determinations of H_2O+, F, and Li, which are often questionable, were done by up-to-date analytical methods. The determinations of water and fluorine are liable to an error of $\leq 20\%$ (Dr. Z. Šulcek[2] pers. comm.). In a few samples, too little material precluded determinations of F and/or H_2O+; in some others, Cs_2O and Rb_2O were included in K_2O.

Recently, many authors base the calculation of mica formulas on the assumption of 24 anions per cell (Gottesmann, 1962; Foster *et al.*, 1963, case (A); Stern, 1966). Formulas of the micas studied were calculated using such a conversion factor

$$K_f = \frac{24}{\Sigma O + F}, \tag{1}$$

where ΣO is the sum of atomic ratios of oxygen and F is the atomic ratio for fluorine. (To obtain formula coefficients, atomic ratios of individual elements [= weight percent divided by atomic weight] are multiplied by K_f.) Many of

2 Chief of the Analytical Laboratory, Ústřední ústav geologický, Praha.

Table 1. *Idealized formulas for some mica end members and varieties*

	Octahedral	Tetrahedral	
Annite	$K_2 Fe^{+2}_6$	Al_2Si_6	$O_{20}(OH,F)_4$
Cryophyllite	a superfluous name for ferroan polylithionite or ferroan trilithionite (ferroan lepidolite)		
Ferroan polylithionite (a variety)	$K_2 Li_{3-4}Fe^{+2}_{1-0}$ (Al, Fe^{+3})$_2$	$Al_{1-0}Si_{7-8}$	$O_{20}(F,OH)_4$
Lithian siderophyllite (a variety)	$K_2 Fe^{+2}_{3-4}Li_{1-0}$ (Al, Fe^{+3})$_2$	$Al_{3-4}Si_{5-4}$	$O_{20}(OH,F)_4$
Muscovite	$K_2 Al_4$	Al_2Si_6	$O_{20}(OH,F)_4$
Phlogopite	$K_2 Mg_6$	Al_2Si_6	$O_{20}(OH,F)_4$
Polylithionite	$K_2 Li_4Al_2$	Si_8	$O_{20}(F,OH)_4$
Protolithionite	defined by Winchell (1942) as $K_2 LiFe^{+2}_4Al$	Al_2Si_6	$O_{20}(F,OH)_4$
	compositions corresponding to this formula have not been found		
Siderophyllite	$K_2 Fe^{+2}_4$(Al, Fe^{+3})$_2$	Al_4Si_4	$O_{20}(OH,F)_4$
Taeniolite	$K_2 Li_2Mg_4$	Si_8	$O_{20}(F,OH)_4$
Trilithionite	$K_2 Li_3Al_3$	Al_2Si_6	$O_{20}(F,OH)_4$
Zinnwaldite	$K_2 Fe^{+2}_{1-3}Li_{3-1}$ (Al, Fe^{+3})$_2$	$Al_{1-3}Si_{7-5}$	$O_{20}(F,OH)_4$

the present analyses, however, report so much water that the corresponding formulas have more than four (OH, F)[3], which has not been verified by structure analyses of the micas (Dr. M. Ross, pers. comm.). Alternate methods of calculation had to be sought if all water is to be accomodated in a cell whose (OH, F) $\leqq 4$.

Water determinations demanding more than four (OH) had been known in hydrous micas and used to be discarded (Hendricks and Ross, 1941; Grim *et al.*, 1951). Brown and Norrish (1952) assumed that oxonium, $(H_3O)^+$, accompanies potassium in the interlayer position and achieved a better agreement between analyses and formulas. Mikheev (1954) calculated oxonium in the formulas of fourteen out of nineteen mica minerals; Pavlishin (1965) calculated 0.08 $(H_3O)^+$ in his "protolithionite". There is direct evidence of the presence of oxonium in layer silicates: Bokii and Arkhipenko (1962) reported oxonium in vermiculite on the basis of an IR spectrum and chemical analysis; White and Burns (1963) used an IR spectrum to detect oxonium in an experimentally treated muscovite; Sclar *et al.* (1965) reported a synthesis ($p = 32$ to 90 kb, $T = 375$ to 525 °C) of a layer silicate (related to talc and phlogopite) that contains $(H_3O)^+$ as the only interlayer cation. The presence of $(H_3O)^+$ in natural micas was postulated by Ross and Evans (1965) on the basis of a study of isomorphism among K-(H_3O)-(NH_4) uranophosphates and uranovanadates[4].

An assumption of the presence of oxonium in natural micas is no worse than an assumption of its absence. A modified conversion factor was derived on the basis of such assumptions: (i) The mica is electrically neutral and has 44 negative and positive charges per cell. (ii) The cell contains twenty oxygens. (iii) The sum

3 Several such cases have been reported: "protolithionite" with $F_{2.56}(OH)_{1.96}$ (Gottesmann, 1962); zinnwaldite no. 1358 with $F_{3.36}(OH)_{1.02}$ (Povilaitis and Organova, 1963); lepidolite with $F_{1.44}(OH)_{2.64}$ (Yakovleva *et al.*, 1965). Nine out of thirteen formulas listed by Němec (1969) have less than twenty oxygens.

4 Ammonium micas have been synthesized (Eugster and Munoz, 1966).

of fluorine and hydroxyl groups is four. (iv) All "empty" interlayer sites are filled with oxonium. (v) The plane of tetrahedral cations is occupied completely by Si, Ti [5], Al, Fe^{+3}, Cr^{+3}. The corresponding equations are:

$$\begin{aligned} o+h+x+v &= K_f \Sigma O \\ h+3x+2v &= K_f H \\ h+f &= 4 \\ i+x &= 2 \\ f &= K_f F \\ i &= K_f I \\ o &= 20, \end{aligned}$$

where lower-case letters denote formula coefficients: f = fluorine; o = oxygen; h = hydroxyl; i = total interlayer cations other than oxonium; x = oxonium; v = "excess water". ΣO is the total of atomic ratios for oxygen; H is the atomic ratio for hydrogen; I is the total of atomic ratios for interlayer cations other than oxonium; F is the atomic ratio for fluorine. By solving we obtain

$$K_f = \frac{42}{F-I+2\Sigma O-H}. \qquad (2)\ [6]$$

Unless an "excess water" term is introduced, there are more equations than unknowns, and the water determinations of very few, if any, mica analyses will match the assumptions. This approach is useful if the H_2O+ determination is missing, as in samples no. 17, 30, and 40. We can assume v = 0, and the resulting factor becomes

$$K_f = \frac{42}{F-I+2\Sigma O'}, \qquad (3)$$

where $\Sigma O'$ represents all oxygen reported in the analysis; *i.e.*, ΣO less the oxygen in H_2O+. Neither H_2O+ nor fluorine were determined in samples no. 33 and 37. The starting equations can be recast to yield

$$K_f = \frac{42}{-I+2\Sigma O''}, \qquad (4)$$

where $\Sigma O''$ represents all oxygen reported in the analysis; *i.e.*, ΣO less oxygen in H_2O+, plus oxygen not deducted for F/2. Again, v is assumed equal to zero, and f and h are not specified by the calculation, yet their sum must be four.

In formulas calculated using factor (2), v may be positive or negative (or zero). Positive v must be interpreted as due to adsorbed water, unless we invoke inaccuracy of the analysis. Negative v may be an indication against assumption (iv) or an indication of the presence of oxygen in hydroxyl & fluorine sites

5 In view of a close geochemical relation of titanium to silicon (Rankama and Sahama, 1950, p. 125) and in view of the role of Ti in micas (Serdyuchenko, 1948), titanium was placed into the tetrahedral sheet. Foster (1960a) placed all Ti into the octahedral sheet. Kovalenko *et al.* (1968) reported that titanium entered both tetrahedral and octahedral sites.

6 The result of Bokii and Arkhipenko's (1962) calculation of the crystallochemical formula of vermiculite, which was questioned by White and Burns (1963), can be duplicated by the use of a conversion factor similar to (2).

Table 2. *Calculation of crystallochemical formula from analysis of sample 2 using four different conversion factors*

Atomic ratios of elements (r_i) are calculated from weight percent ($\%_i$) of oxides $(R_mO_n)_i$ as $r_i = \frac{m_i\ \%_i}{m_i a_i + n_i a_O}$, where a_i is the atomic weight of i-th element and a_O the atomic weight of oxygen. The atomic ratio for oxygen is $r_O = \sum_i \left(\frac{n_i\ \%_i}{m_i a_i + n_i a_O}\right) - \frac{r_F}{2}$. From the atomic ratios thus obtained (ΣO for oxygen, F for fluorine, H for hydrogen, I for interlayer cations other than oxonium), conversion factors are calculated using the following formulas:

$$K_f = \frac{24}{\Sigma O + F} \quad (1)$$

$$K_f = \frac{42}{F - I + 2\Sigma O - H} \quad (2)$$

$$K_f = \frac{68}{3\Sigma O + 2F - H} \quad (5)$$

$$K_f = \frac{26}{\Sigma O + I + F} \quad (6)$$

Element	Sample 2		Formula coefficients calculated using conversion factor			
	analysis (wt.% of oxides)	atomic ratio	(1)	(2)	(5)	(6)
Interlayer						
K	7.40	0.157126	1.40	1.40	1.41	1.42
Rb	0.93	0.009949	0.09	0.09	0.09	0.09
Cs	0.024	0.000170	+	+	+	+
Na	0.28	0.009033	0.08	0.08	0.08	0.08
Ca	0.28	0.004993	0.04	0.04	0.04	0.05
H_3O	—	—	—	0.39	0.10	0.36
Octahedral						
Li	1.24	0.082999	0.74	0.74	0.74	0.75
Fe^{+2}	19.01	0.264579	2.36	2.35	2.37	2.39
Mg	2.32	0.057540	0.51	0.51	0.52	0.52
Mn^{+2}	0.57	0.008036	0.07	0.07	0.07	0.07
Al	22.16	0.434765	1.59	1.57	1.62	1.72
Fe^{+3}	2.85	0.035692	0.32	0.32	0.32	0.32
Tetrahedral						
Al	—	—	2.29	2.30	2.27	2.21
Si	37.90	0.631246	5.63	5.62	5.65	5.71
Ti	0.73	0.009136	0.08	0.08	0.08	0.08
O	—	2.608397	19.70	20.00	20.00	20.00
OH	—	—	0.30	—	—	—
F	1.60[a]	0.084211	0.75	0.75	0.75	0.76
OH	3.59[b]	0.398535[b]	3.25	3.25	3.25	2.53
O	—	—	—	—	—	0.71
		v	—	−0.44	—	—
		Σ oct	5.59	5.56	5.64	5.77
		Σ (+)oct	12.35	12.27	12.48	12.83
		Σ (+)	43.71	44.01	43.97	44.67
		Σ (−)	43.70	44.00	44.00	44.71
		A	0.379	0.379	0.378	0.379
		A′	0.233	0.234	0.233	0.234
		B	0.827	0.826	0.824	0.826
		C	0.256	0.256	0.260	0.257
		Q	0.209	0.207	0.213	0.224
		K_f	8.913	8.896	8.953	9.047
		D_x	3.040	3.060	3.052	3.081

(oxy-micas). In the first case, the plane of interlayer cations may be underoccupied, and the equations

$$\begin{aligned} o+h+x &= K_f \Sigma O \\ h+3x &= K_f H \\ h+f &= 4 \\ f &= K_f F \\ o &= 20 \end{aligned}$$

yield

$$K_f = \frac{68}{3\Sigma O + 2F - H}, \tag{5}$$

which is analogous to Brown and Norrish's (1952) factor (modified for fluorine). Formulas of oxonium-bearing oxy-micas can be calculated using a K_f derived from the following equations:

$$\begin{aligned} o+h+f &= 24 \\ o+h+x &= K_f \Sigma O \\ h+3x &= K_f H \\ i+x &= 2 \\ f &= K_f F \\ i &= K_f I. \end{aligned}$$

The factor is

$$K_f = \frac{26}{\Sigma O + I + F}. \tag{6}$$

Unless it is possible to perform precise and accurate density measurements and/or to determine the quantities of oxygen in (OH, F) sites and of oxonium, there are no grounds to prefer either (5) or (6). Conversion factor (6) was used for formulas whose calculation with (2) gave $v < 0$.

Some of the resulting formulas have negative oxonium coefficients. These correspond to micas whose Rb and Cs were included in the determination of potassium (Table 4). Due to higher atomic weights of Rb and Cs, the apparent coefficient for K is larger than the sum of coefficients K + Rb + Cs. The sum of interlayer cations other than oxonium thus may exceed two. An exception is samples no. 1 and 45 (Stevens, 1938), for which no cause is suggested.

Formulas calculated using different conversion factors plot close to each other in critical composition diagrams; thus there is almost no danger that the method of calculation introduces bias into the correlation of chemical composition and physical properties. Sample calculation of a crystallochemical formula by factors (1), (2), (5), and (6) is given in Table 2.

Explanations to Table 2:

+ = coefficient < 0.005. — = not present. v = "excess water"; see 2.2 for definition. Σoct = octahedral occupancy. $\Sigma(+)$oct = octahedral positive charges. $\Sigma(+)$ = total positive charges. $\Sigma(-)$ = total negative charges. D_x = calculated density. For definition of ratios A, A', B, C, and Q see 2.3 or Table 4.

[a] Determined as F^-.

[b] Determined as H_2O+; the atomic ratio refers to hydrogen.

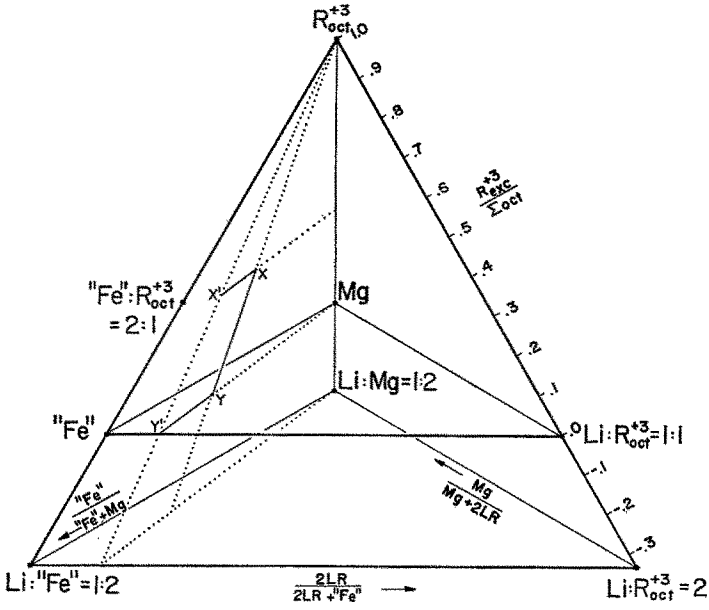

Fig. 2. A pyramid for plotting atomic octahedral compositions of Li-Fe-Mg-Al micas. "Fe" = $Fe^{+2}+Mn^{+2}$; R^{+3}_{oct} is the sum of octahedral trivalent cations; $R^{+3}_{exc}=R^{+3}_{oct}-Li$; LR is Li or R^{+3}_{oct}, whichever is smaller; Σoct is the sum of octahedral cations. If we plot the ratios $2LR/(2LR+"Fe")$ and $R^{+3}_{exc}/\Sigma oct$ only, we obtain a projection of compositions onto the front face of the pyramid: points X and Y project as X' and Y'. Projections onto any other face can be obtained in an analogous manner

2.3. Graphical Representation

Compositions of the micas studied were classified according to octahedral cations[7], as had been done by most authors (Foster, 1960a, 1960b; Gottesmann, 1962; Povilaitis and Organova, 1963; Stern, 1966). There are seven cations in the octahedral sheets of the micas studied: Li, Fe^{+2}, Mg, Mn^{+2}, Al, Fe^{+3}, and Cr^{+3}. The number of octahedral vacancies was disregarded in composition plots. The following symbols were introduced: Mg for Mg; "Fe" for $Fe^{+2}+Mn^{+2}$; R^{+3}_{oct} for octahedral $Al+Fe^{+3}+Cr^{+3}$; and Li for Li. These four quantities define three ratios:

$$A=\frac{2\,LR}{2\,LR+"Fe"}, \quad B=\frac{"Fe"}{"Fe"+Mg}, \quad C=\frac{Mg}{Mg+2\,LR},$$

where LR is Li or R^{+3}_{oct}, whichever is smaller. The relation between R^{+3}_{oct} and Li can be converted into another parameter, $Q=R^{+3}_{exc}/\Sigma oct$; R^{+3}_{exc} is defined as $R^{+3}_{oct}-Li$; Σoct is the sum of octahedral cations. Values of individual ratios are plotted in a pyramid (Fig. 2).

Fig. 3 shows the plot of the idealized formulas of Table 1. Phlogopite, annite, "protolithionite", zinnwaldite, and trilithionite lie in a horizontal plane at

7 For convenience, elements involved in micas are referred to as cations or anions, although their bonding may not be purely ionic.

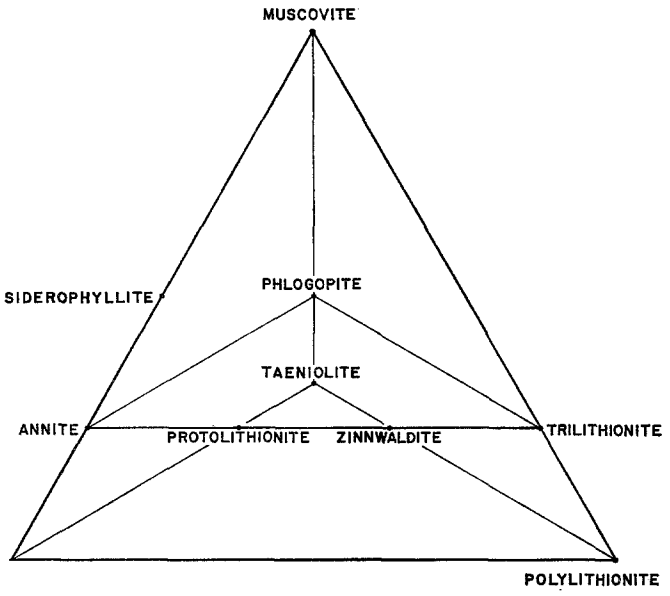

Fig. 3. Nomenclature of mica end members plotting in the pyramid of Fig. 2. The species are plotted according to the formulas listed in Table 1, zinnwaldite is plotted as the middle of the range given. The bottom left corner represents the formula $K_2Li_2Fe_4^{+2}Si_8O_{20}(OH, F)_4$ not known from nature

$Q=0$, their Li being equal to R_{oct}^{+3}. Polylithionite, taeniolite, and its iron analog define another horizontal plane at $Q=-\frac{1}{3}$, with excess of Li over R_{oct}^{+3}. In cation-deficient micas, cases with $Q<-\frac{1}{3}$ are possible. Containing no lithium, muscovite occupies the apex. Siderophyllite lies at $Q=\frac{1}{3}$.

The value of Q is proportionate to R_{exc}^{+3}. Both do or may increase due to: octahedral vacancies created by replacement R_{oct}^{+1}, $R_{oct}^{+2} \rightarrow R_{oct}^{+3}$; tetrahedral substitution $R^{+4} \rightarrow R^{+3}$; anionic substitution $OH, F \rightarrow O$; interlayer vacancies. Bivalent cations in interlayer position may decrease R_{exc}^{+3} and Q. As all these substitutions do not necessarily depend on Σoct, the value of Q does not make it possible to draw a line between "dioctahedral" and "trioctahedral" micas. This is illustrated by polylithionite ($Q=-\frac{1}{3}$), annite ($Q=0$), and siderophyllite ($Q=\frac{1}{3}$), all strictly "trioctahedral". However, "dioctahedral" micas lie close to or at the apex of the pyramid ($Q=1$), and "trioctahedral" micas accumulate near and at its base.

This graphical system is similar to Foster's (1960b). The use of ratios permits one to construct easily projections of octahedral compositions onto any one of the four surface planes (Fig. 2). The system differs from the one based on Stevens' (1938) calculation of mica components, which was used by Tröger (1962) for lithium-iron micas. Stevens' calculation is based on octahedral cations and tetrahedral R^{+4}. Tetrahedral R^{+4} varies with both octahedral vacancies and octahedral Li; in Stevens' (1938) approach the effects of both are scrambled

in the calculation of polylithionite component and, consequently, of muscovite and trilithionite components. The system of Figs. 2 and 3 differs also from Munoz's (1968), in which compositions of lepidolites are expressed in terms of muscovite (MS), trilithionite (TL), and polylithionite (PL). Munoz's triangle may not be a plot of three composition parameters; it can be duplicated by plotting two parameters, such as octahedral occupancy (not a compositional parameter *sensu stricto*) and a function of R_{oct}^{+3}: Li. Similar graphs result from a coordinate transformation of several Foster's (1960b) two-parameter diagrams, in which most points fall between lines joining plots of ideal formulas of muscovite, trilithionite, and polylithionite. The triangle MS-TL-PL also poses a problem with nomenclature: A mica $K_2Li_{\frac{8}{3}}Al_{\frac{8}{3}}Al_{\frac{2}{3}}Si_{\frac{22}{3}}O_{20}(F, OH)_4$, which plots as 66.6 mol% PL, 33.3% MS, and 0% TL, can be considered a *cation-deficient trilithionite*. This name is supported by the distribution of $2M_2$ structure (typical for trilithionite) in Munoz's (1968) triangle, where it converges to a line with $Li = R_{oct}^{+3}$. Also Franzini's (1969) model of trilithionite structure allows vacancies. Unless the above proves false, micas with no Fe^{+2}, Mn^{+2}, Mg and with $Li = R_{oct}^{+3}$ should be termed trilithionite. Hence it is legitimate to project the triangle MS-PL-TL onto the muscovite-polylithionite join, as had been done by Foster (1960b) (see also Fig. 3).

2.4. Results

Analyses of the micas studied are given in Table 3, crystallochemical formulas in Table 4. For graphical plots, octahedral compositions were expressed by A, B, C, and Q.

In the micas studied, lithium and iron predominate among large octahedral cations (Li, Fe^{+2}, Mg, Mn^{+2}); aluminum prevails among small ones (Al, Fe^{+3}, Cr^{+3}). The phlogopite component is subordinate, as follows from a projection of compositions onto the base of the pyramid (Fig. 4). Thus the compositions of the given set of lithium-iron micas can be reasonably approximated by a projection onto the front face of the pyramid (Fig. 5).

The magnesium content of lithium-iron micas may be a function of the composition of their parent rocks: Greisens contain no magnesium minerals, and their micas are poor in Mg; magnesium is higher in sample no. 12, which comes from a skarn rich in Mg. However, lepidolites no. 41, 42, 43 are almost Mg-free, although they come from pegmatites that penetrate serpentine bodies and were soaked with low-temperature Mg-rich solutions (Dr. P. Černý, pers. comm.). It appears that the crystal chemistry of the micas *and* the availability of Mg determine the quantity of Mg that enters the mica.

The distribution of points in Fig. 5 can be approximated equally well by siderophyllite-polylithionite and siderophyllite-trilithionite joins. Crystallographic data indicate octahedral ordering of lithium-iron micas (Rieder, 1968a) that can be obeyed by micas on the siderophyllite-polylithionite join and not on the siderophyllite-trilithionite or annite-trilithionite joins. The points in Fig. 5 were therefore projected from the muscovite apex onto the siderophyllite-polylithionite join, and the resulting projection was used as the composition axis in

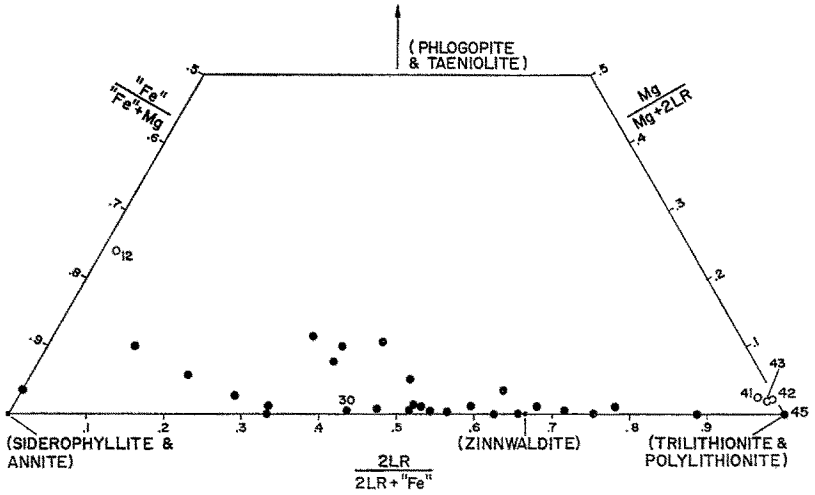

Fig. 4. Octahedral compositions of lithium-iron micas projected onto the base of the pyramid of Fig. 2. Solid circles mark octahedrally ordered micas, open circles, micas with other octahedral arrangements. The numbers refer to sample numbers (Table 3). Small labeled circles represent end members

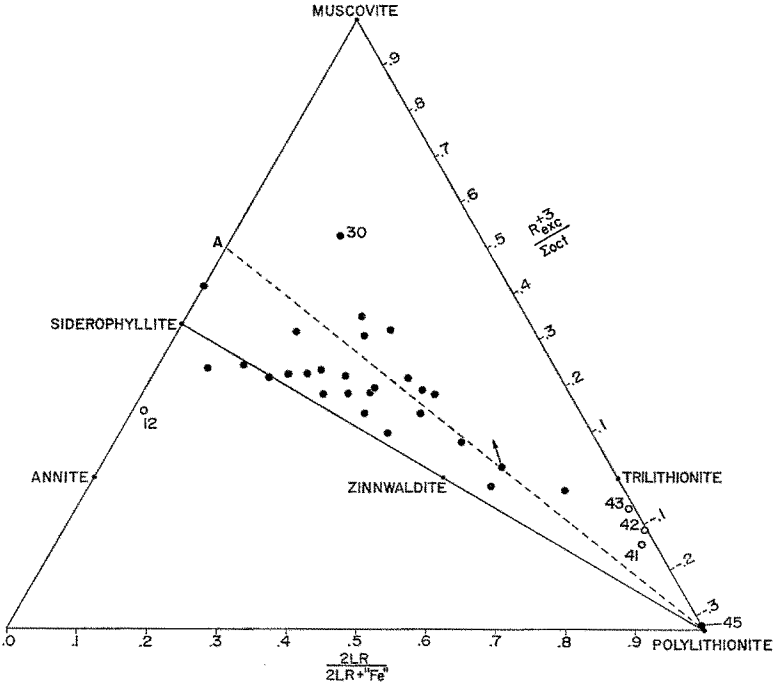

Fig. 5. Octahedral compositions of lithium-iron micas projected onto the front face of the pyramid of Fig. 2. The broken line combining point A ($K_2Fe_2^{+2}Al_2Si_8O_{20}(OH, F)_4$) with polylithionite represents idealized tetrasilicic formulas with octahedral vacancies (see 2.4.1). The arrow shows the "composition" of a mica contaminated with SiO_2; for more detail see 2.4.2. Other symbols as in Fig. 4

Table 3. *Chemical analyses of natural lithium-iron micas arranged in order of increasing values of* $A' = \frac{\text{LR}}{\text{LR}+\text{"Fe"}}$ [a]

	Sample No.						
	44	12	8	7	18	13	31
SiO_2	39.60	32.72	35.46	35.38	34.45	37.88	37.87
TiO_2	0.21	1.25	0.16	0.10	0.31	0.12	0.18
Al_2O_3	22.80	15.03	19.72	20.00	18.87	20.97	23.17
Ga_2O_3	[b]	n.d.	n.d.	n.d.	n.d.	n.d.	n.d.
Cr_2O_3	[b]	—	—	—	0.41	—	—
Fe_2O_3	0.79	4.99	3.18	3.90	5.30	2.39	2.60
FeO	20.98	27.16	24.73	22.50	21.95	21.04	18.60
MnO	0.29	0.16	0.62	0.53	0.84	0.74	0.34
MgO	0.46	4.97	1.81	1.02	0.52	0.25	tr.
CaO	1.52	0.56	0.62	0.84	0.27	0.34	0.64
Li_2O	0.00	0.08	0.38	0.66	0.95	1.12	0.93
Na_2O	tr.	0.14	0.12	0.16	0.88	0.24	0.50
K_2O	8.95	6.46	6.24	8.00	9.34	7.92	9.68
Rb_2O	[b]	0.16	0.49	0.70	[c]	0.70	[c]
Cs_2O	[b]	0.017	0.022	0.029	[c]	0.031	[c]
Tl_2O	[b]	n.d.	n.d.	n.d.	n.d.	n.d.	n.d.
P_2O_5	[b]	0.32	0.08	tr.	0.05	0.03	0.18
CO_2	[b]	—	—	—	tr.	—	tr.
H_2O^+	2.93	4.44	5.64	4.23	3.11	4.40	2.84
H_2O^-	0.24	0.32	0.11	0.11	0.78	0.22	0.29
F	2.03	0.94	1.55	4.04	3.90	4.20	2.41
S	[b]	0.10	tr.	tr.	0.03	0.06	0.02
	100.80	99.817	100.932	102.199	101.96	102.651	100.25
$2F=O$	−0.85	−0.39	−0.65	−1.70	−1.64	−1.76	−1.01
Σ	99.95	99.427	100.282	100.499	100.32	100.891	99.24
Conversion factor							
Value	9.053	9.708	9.335	9.434	9.629	9.214	9.155
Number	6	6	2	2	2	2	2
Analyst	1	2	2	2	3 and 4	2	3 and 4

— = not present. n.d. = not determined. tr. = traces.

[a] LR is formula coefficient for Li or R^{+3}_{oct}, whichever is smaller; "Fe" is the sum of formula coefficients for Fe^{+2} and Mn^{+2}; for values of $\frac{\text{LR}}{\text{LR}+\text{"Fe"}}$ see Table 4.

[b] Not determined or not present.

[c] Included in K_2O.

[d] In addition to the oxides given, the analysis reports 1.52% Nb_2O_5; prior to calculation of the crystallochemical formula, niobium pentoxide was subtracted as columbite, $(Fe, Mn)Nb_2O_6$.

Analysts: 1 = N. Sahlbom (in Nockolds and Richey, 1939). 2 = M. Huka. 3 = D. Kučerová. 4 = J. Obermajer. 5 = P. Povondra. 6 = L. Minařík. 7 = R. E. Stevens (Stevens, 1938).

Localities:

1. Cínovec Mine, 2nd level. In a vein with quartz and wolframite. Coll. M. Štemprok.
2. Krupka, Barbora gallery dump. In a pegmatite with quartz I, feldspar I, and clay minerals. Coll. L. Žák.

2	23	3	30	4	6	33	10	14
37.90	37.44	38.38	43.37	40.08	41.32	39.64	39.74	44.36
0.73	1.23	0.49	0.20	0.06	0.45	0.04	0.08	0.06
22.16	19.19	20.73	21.91	22.34	20.86	21.33	22.11	22.65
n.d.	n.d.	n.d.	n.d.	n.d.	n.d.	n.d.	n.d.	n.d.
—	—	—	—	—	—	—	—	—
2.85	5.27	2.30	6.41	2.53	1.68	5.28	1.80	1.61
19.01	16.80	17.89	9.80	17.14	16.29	11.87	17.53	13.47
0.57	0.57	0.62	0.13	0.57	0.45	0.30	0.38	0.32
2.32	1.40	2.01	0.03	0.14	2.13	0.10	0.11	0.24
0.28	0.13	0.22	0.66	0.28	0.28	0.50	0.31	0.89
1.24	1.25	1.40	0.79	1.66	1.60	1.36	2.00	1.56
0.28	0.60	0.18	0.50	0.24	0.20	0.42	0.22	0.24
7.40	9.40	7.96	7.97	8.36	7.80	8.42	8.16	8.16
0.93	c	0.93	c	0.98	0.71	c	0.86	0.73
0.024	c	0.024	c	0.025	0.019	c	0.018	0.018
n.d.	n.d.	n.d.	n.d.	n.d.	n.d.	n.d.	n.d.	n.d.
tr.	0.06	tr.	0.28	tr.	tr.	0.08	tr.	0.04
—	tr.	—	—	—	—	—	—	—
3.59	2.65	3.67	n.d.	3.99	3.57	n.d.	3.07	3.12
0.32	0.89	0.40	2.22	0.08	0.12	2.12	0.25	0.12
1.60	4.16	4.70	2.80	3.85	3.70	n.d.	5.00	3.15
tr.	n.d.	tr.	—	0.05	0.08	—	tr.	tr.
101.204	101.04	101.904	97.07	102.375	101.259	91.46	101.638	100.738
−0.67	−1.75	−1.97	−1.18	−1.62	−1.55		−2.10	−1.32
100.534	99.29	99.934	95.89	100.755	99.709		99.538	99.418
9.047	9.294	9.121	8.816	8.934	8.842	9.258	8.901	8.670
6	2	2	3	2	2	4	2	6
2	3	2	2 and 4	2	2	2	2	2

3. Krupka, Barbora gallery dump. In a pegmatite with quartz, orthoclase, and clay minerals. Coll. L. Žák.
4. Krupka, Barbora gallery dump. In a vein with topaz, quartz, fluorite, and clay minerals. Coll. L. Žák.
5. Krupka, Barbora gallery dump. In a vein with quartz, fluorite, and chlorite (?). Coll. F. Kern.
6. Krupka, Václav gallery dump. In a vein cutting gneiss; with quartz, fluorite, and molybdenite. Coll. B. Mühlstein.
7. Krupka, Nový Lukáš gallery dump. Vein (?) accumulation with K-spar, fluorite, and quartz. Coll. L. Žák.
8. Krupka, Nový Lukáš gallery dump. Vein (?) accumulation with quartz. Coll. L. Žák.
9. Krupka, drill KV 9, depth 347 meters. Mica aggregate next to albitized white granite. Coll. L. Žák and M. Štemprok.
10. Krupka, drill KV 9, depth 466 meters. Mica aggregate next to greisen. Coll. L. Žák.
12. Budeč near Žd'ár nad Sázavou. In a skarn with quartz and pyrite. Coll. F. Čech.

Table 3 (continued)

	Sample No.						
	29	9	35	38	40	5	37
SiO_2	37.82	41.40	39.52	43.59	42.86	43.90	41.20
TiO_2	0.16	0.05	0.17	0.07	0.16	0.20	0.08
Al_2O_3	23.06	22.21	19.45	23.65	21.89	21.27	22.53
Ga_2O_3	n.d.	n.d.	n.d.	n.d.	n.d.	n.d.	n.d.
Cr_2O_3	—	—	2.25	—	—	—	—
Fe_2O_3	2.73	2.54	1.35	2.82	2.78	2.01	2.89
FeO	16.25	15.52	16.60	10.78	11.84	13.29	11.48
MnO	0.30	0.55	0.79	0.58	0.73	0.02	0.47
MgO	0.23	0.09	0.09	0.17	tr.	0.77	tr.
CaO	0.13	0.67	tr.	0.27	0.51	0.42	0.74
Li_2O	1.96	1.98	2.35	1.75	2.19	2.46	2.36
Na_2O	0.76	0.30	0.70	0.33	0.26	0.36	0.22
K_2O	9.68	8.32	9.60	10.58	9.85	7.76	8.69
Rb_2O	c	0.92	c	c	c	0.74	c
Cs_2O	c	0.028	c	c	c	0.023	c
Tl_2O	n.d.	n.d.	n.d.	n.d.	n.d.	n.d.	n.d.
P_2O_5	0.09	tr.	0.06	0.03	0.04	0.03	0.10
CO_2	tr.	—	tr.	tr.	—	—	—
H_2O^+	3.06	2.85	2.71	3.24	n.d.	3.08	n.d.
H_2O^-	0.96	0.04	0.78	0.43	0.96	0.21	1.15
F	5.10	3.52	6.45	3.75	5.20	5.00	n.d.
S	tr.	tr.	0.03	tr.	—	tr.	—
	102.29	100.988	102.90	102.04	99.27	101.543	91.91
$2F=O$	−2.15	−1.48	−2.72	−1.58	−2.18	−2.10	
Σ	100.14	99.508	100.18	100.46	97.09	99.443	
Conversion factor							
Value	9.152	8.834	9.193	8.661	8.826	8.655	8.968
Number	2	6	2	2	3	2	4
Analyst	3 and 4	2	3 and 4	3 and 4	2 and 4	2	2

Localities (continued):

13. Krupka, Martin gallery dump. Vein (?) accumulation with quartz, feldspar, and clay minerals. Coll. M. Rieder.
14. Krupka, Barbora gallery dump. In greisen with quartz and native Bi. Coll. L. Žák.
15. Krupka, Večerní hvězda gallery dump. In greisen with quartz. Coll. M. Rieder.
16. Cínovec, drill Cs-1, depth 609—609.8 meters. In granite. Coll. M. Štemprok.
17. Krupka, drill KV 16, depth 392.5 meters. In a vein cutting granite. Coll. M. Štemprok.
18. Krupka, Lukáš vein, Martin gallery. In a vein with quartz, clay minerals, and iron oxides. Coll. M. Štemprok and B. Karbula.
22. Cínovec, drill Cs-1, depth 262—262.4 meters. In albitized granite (quartz, K-spar, albite, and sericite). Coll. M. Štemprok,
23. Cínovec, drill Cs-1, depth 778.5 meters. In sericitized granite (quartz, feldspar, sericite). Coll. M. Štemprok.
29. Ehrenfriedersdorf, Sauberg Mine, 5th level, 2nd level drift, Prinzlergangzug (Prinzler vein swarm), stope no. 5408. In a "pegmatite" with quartz. Coll. M. Rieder.
30. Ehrenfriedersdorf, Sauberg Mine, 2nd level, stope no. 510A. In "Stockscheider" with quartz, feldspar, and a light mica. Coll. M. Rieder.
31. Geyer, dump. Mica aggregate with clay minerals, quartz, and arsenopyrite. Coll. M. Rieder.

15	16	1	22	17	41	43	42	45
43.12	44.16	46.08	45.51	48.08	52.80	51.45	51.40	59.56
0.03	0.20	0.05	0.24	0.09	n.d.	n.d.	n.d.	0.48
22.16	22.24	19.68	20.59	18.03	19.94	22.62	21.31	12.04
n.d.	n.d.	n.d.	n.d.	n.d.	—	0.0098	0.0035	[b]
—	—	—	—	—	—	0.0005	0.0007	—
4.35	2.02	1.15	1.51	2.43	0.379	0.160	0.133	0.1
11.00	11.49	10.38	9.20	4.24	0.055	0.036	0.024	0.43
0.39	0.62	1.20	0.53	0.62	0.88	0.51	0.19	0.02
0.22	0.13	tr.	0.30	tr.	0.63	0.53	0.60	0.33
0.72	0.56	0.53	0.27	0.77	0.11	0.20	0.13	tr. 4
2.54	3.18	3.80	3.66	4.34	5.91	5.42	5.72	7.26
0.22	0.32	0.18	0.60	0.69	0.26	0.26	0.13	0.53
9.16	5.92	10.88	9.68	9.66	9.00	9.09	9.74	11.05
0.92	1.28	1.08	[c]	[c]	1.36	1.69	1.25	1.14
0.026	0.061	0.019	[c]	[c]	0.75	0.94	1.00	—
n.d.	n.d.	n.d.	n.d.	n.d.	—	0.0071	0.0091	[b]
0.02	0.02	tr.	0.02	0.03	n.d.	n.d.	n.d.	[b]
—	—	—	n.d.	—	n.d.	n.d.	n.d.	[b]
2.79	3.85	2.26	1.90	n.d.	2.85	2.36	3.14	0.47
0.17	0.44	0.18	1.21	3.45	—	0.84	0.54	0.73
4.95	6.10	5.30	7.45	7.20	7.07	7.40	7.08	7.73
tr.	tr.	0.08	n.d.	—	n.d.	n.d.	n.d.	[b]
102.786	102.591	102.849	102.67	99.63	101.994	103.5234	102.4003	103.43[d]
—2.08	—2.56	—2.23	—3.14	—3.03	—2.98	—3.11	—2.98	—3.26
100.706	100.031	100.619	99.53	96.60	99.014	100.4134	99.4203	100.17
8.629	8.545	8.633	8.668	8.756	8.142	8.123	8.232	8.067
2	2	2	2	3	2	2	2	2
2	2	2	3 and 4	2 and 4	5 and 6	5 and 6	5 and 6	7

33. Geyer, dump (drill core). Accumulated rock-forming mica in greisen; with quartz and feldspar. Coll. M. Rieder.
35. Altenberg Mine, 7th level. In "Stockscheider" with topaz (var. pycnite) and quartz. Coll. M. Rieder.
37. Vysoký Kámen near Slavkov. In an outcropping greisen; with quartz, hematite(?), feldspar (?), cassiterite, and wolframite. Coll. M. Rieder.
38. Krásno near Slavkov, Hubský peň (Huberstock), 4th level. Drift no. P946. In cavities in vein; grown on quartz and clay minerals (?). Coll. M. Rieder.
40. Sadisdorf Mine dump. Accumulation with quartz and sericite or clay minerals. Coll. L. Žák.
41. Biskupice near Hrotovice. In a lithium pegmatite with albite and rubellite. Coll. P. Černý.
42. Radkovice near Hrotovice. Mica accumulation in a lithium pegmatite. Coll. P. Černý.
43. Radkovice near Hrotovice. In a lithium pegmatite with albite, quartz, and rare topaz. Coll. P. Černý.
44. Newcastle Co. Down (Northern Ireland). In a greisen vein with topaz (Nockolds and Richey, 1939).
45. Kangerdluarsuk, Julianehaab District, Greenland (Stevens, 1938).

Table 4. *Crystallochemical formulas of natural lithium-iron micas arranged in order of increasing values of* $A' = \frac{LR}{LR + \text{“Fe”}}$ [a]

Element	Sample No.						
	44	12	8	7	18	13	31
Interlayer							
K	1.72	1.33	1.24	1.61	1.91	1.55	1.88
Rb	[b]	0.02	0.05	0.07	[c]	0.07	[c]
Cs	[b]	+	+	+	[c]	+	[c]
Na	+	0.04	0.03	0.05	0.27	0.07	0.15
Ca	0.25	0.10	0.08	0.15	0.04	0.05	0.07
H_3O	0.03	0.51	0.60	0.12	−0.22	0.26	−0.10
Octahedral							
Li	0.00	0.05	0.24	0.42	0.61	0.69	0.60
Fe^{+2}	2.64	3.67	3.22	2.97	2.94	2.69	2.37
Mg	0.10	1.20	0.42	0.24	0.12	0.05	+
Mn^{+2}	0.04	0.02	0.08	0.07	0.11	0.09	0.04
Al	2.04	0.30	1.19	1.30	1.12	1.63	1.95
Fe^{+3}	0.09	0.61	0.36	0.46	0.64	0.27	0.30
Cr^{+3}	[b]	—	—	—	0.05	—	—
Tetrahedral							
Al	2.01	2.56	2.44	2.41	2.44	2.16	2.21
Si	5.97	5.29	5.54	5.58	5.52	5.83	5.77
Ti	0.02	0.15	0.02	0.01	0.04	0.01	0.02
O	20.00	20.00	20.00	20.00	20.00	20.00	20.00
F	0.97	0.48	0.76	2.01	1.98	2.04	1.16
OH	2.85	3.26	3.24	1.99	2.02	1.96	2.84
O	0.18	0.26	—	—	—	—	—
v	—	—	0.43	1.05	0.98	0.90	0.17
Σoct	4.91	5.85	5.51	5.46	5.59	5.42	5.26
Σ(+)oct	11.95	12.56	12.33	12.26	12.38	12.05	12.17
A	0.000	0.026	0.127	0.216	0.286	0.332	0.332
A′	0.000	0.013	0.068	0.121	0.167	0.199	0.199
B	0.964	0.755	0.887	0.927	0.962	0.982	1.000
C	1.000	0.923	0.467	0.222	0.090	0.035	0.000
Q	0.415	0.147	0.238	0.245	0.215	0.223	0.314

+ = coefficient < 0.005. — = not present. v = “excess water”; see 2.2 for definition. Σ oct = octahedral occupancy. Σ (+) oct = octahedral positive charges.

$$A = \frac{2\,LR}{2\,LR + \text{“Fe”}}\ ^{a} \qquad C = \frac{Mg}{Mg + 2\,LR}\ ^{a}$$

$$A' = \frac{LR}{LR + \text{“Fe”}}\ ^{a} \qquad Q = R^{+3}_{exc}/\Sigma\ oct,\ (R^{+3}_{exc} = R^{+3}_{oct} - Li)$$

$$B = \frac{\text{“Fe”}}{\text{“Fe”} + Mg}\ ^{a}$$

Elements found in traces and elements deducted as impurities are not shown in this table.

2	23	3	30	4	6	33	10	14
1.42	1.85	1.54	1.50	1.59	1.47	1.65	1.55	1.50
0.09	[c]	0.09	[c]	0.09	0.07	[c]	0.08	0.07
+	[c]	+	[c]	+	+	[c]	+	+
0.08	0.18	0.05	0.14	0.07	0.06	0.13	0.06	0.07
0.05	0.01	0.03	0.05	0.04	0.04	0.07	0.05	0.14
0.36	−0.04	0.29	0.31	0.21	0.36	0.15	0.26	0.22
0.75	0.78	0.86	0.47	0.99	0.95	0.84	1.20	0.91
2.39	2.17	2.28	1.20	2.13	2.00	1.53	2.17	1.63
0.52	0.32	0.46	0.01	0.03	0.47	0.02	0.25	0.05
0.07	0.07	0.08	0.02	0.07	0.06	0.04	0.05	0.04
1.72	1.43	1.61	2.17	1.90	1.76	1.98	1.77	2.27
0.32	0.61	0.26	0.71	0.28	0.18	0.61	0.21	0.17
—	—	—	—	—	—	—	—	—
2.21	2.07	2.11	1.62	2.02	1.86	1.89	2.10	1.58
5.71	5.79	5.84	6.36	5.97	6.09	6.11	5.89	6.41
0.08	0.14	0.05	0.02	0.01	0.05	+	0.01	0.01
20.00	20.00	20.00	20.00	20.00	20.00	20.00	20.00	20.00
0.76	2.03	2.26	1.30	1.81	1.72	[d]	2.34	1.44
2.53	1.97	1.74	2.70	2.19	2.28	[d]	1.66	2.33
0.71	—	—	—	—	—	—	—	0.23
—	0.44	0.57	—	0.59	0.08	—	0.30	—
5.77	5.38	5.55	4.58	5.40	5.42	5.02	5.65	5.07
12.83	12.02	12.11	11.57	11.99	11.83	11.79	12.08	11.67
0.379	0.411	0.422	0.435	0.474	0.480	0.517	0.519	0.521
0.234	0.259	0.267	0.278	0.311	0.316	0.349	0.350	0.352
0.826	0.875	0.837	0.992	0.987	0.814	0.987	0.899	0.971
0.257	0.170	0.211	0.011	0.015	0.198	0.012	0.094	0.027
0.224	0.234	0.182	0.526	0.220	0.183	0.349	0.138	0.307

[a] LR is formula coefficient for Li or R^{+3}_{oct}, whichever is smaller; "Fe" is the sum of formula coefficients for Fe^{+2} and Mn^{+2}.

[b] The corresponding oxide was not determined or is not present.

[c] Rb_2O and Cs_2O were included in K_2O.

[d] Cannot be calculated from the analysis; see 2.2.

Table 4 (continued)

Element	Sample No.							
	29	9	35	38	40	5	37	15
Interlayer								
K	1.88	1.56	1.87	1.94	1.85	1.43	1.66	1.68
Rb	c	0.09	c	c	c	0.07	c	0.08
Cs	c	+	c	c	c	+	c	+
Na	0.22	0.09	0.21	0.09	0.07	0.10	0.06	0.06
Ca	+	0.11	+	0.04	0.07	0.06	0.10	0.11
H_3O	−0.10	0.15	−0.08	−0.07	0.01	0.34	0.18	0.07
Octahedral								
Li	1.20	1.17	1.45	1.01	1.29	1.43	1.42	1.47
Fe^{+2}	2.07	1.91	2.12	1.30	1.45	1.60	1.43	1.32
Mg	0.05	0.02	0.02	0.04	+	0.16	+	0.05
Mn^{+2}	0.04	0.07	0.10	0.07	0.09	+	0.06	0.05
Al	1.92	1.95	1.58	2.31	2.11	1.98	2.12	1.97
Fe^{+3}	0.31	0.28	0.16	0.31	0.31	0.21	0.32	0.47
Cr^{+3}	—	—	0.27	—	—	—	—	—
Tetrahedral								
Al	2.22	1.90	1.93	1.71	1.68	1.64	1.84	1.79
Si	5.76	6.09	6.05	6.28	6.30	6.34	6.15	6.21
Ti	0.02	0.01	0.02	0.01	0.02	0.02	0.01	+
O	20.00	20.00	20.00	20.00	20.00	20.00	20.00	20.00
F	2.46	1.63	3.12	1.81	2.42	2.28	d	2.25
OH	1.54	2.34	0.88	2.19	1.58	1.72	d	1.75
O	—	0.03	—	—	—	—	—	—
v	0.95	—	1.06	2.15	—	0.11	—	0.36
Σ oct	5.59	5.40	5.70	5.04	5.25	5.38	5.35	5.33
Σ (+) oct	12.21	11.86	11.96	11.69	11.63	11.52	11.72	11.63
A	0.532	0.542	0.566	0.596	0.626	0.641	0.656	0.682
A′	0.362	0.372	0.395	0.425	0.456	0.472	0.488	0.517
B	0.977	0.990	0.991	0.972	1.000	0.909	1.000	0.965
C	0.020	0.008	0.007	0.019	0.000	0.053	0.000	0.017
Q	0.184	0.196	0.098	0.319	0.215	0.141	0.191	0.182

several of the figures to follow. The points in this projection are arranged according to

$$A' = \frac{LR}{LR + \text{“Fe”}}; \quad A' = \frac{A}{2 - A}.$$

Fig. 6 shows that the unit cell of ordered lithium-iron micas contains approximately two small cations and never more than four large cations, as required by the model of their structure. A prediction of the structure from Fig. 6 may not be reliable, though. The number of “Fe” cations in mica no. 12 will obviously prohibit ordering, but octahedral cations of lepidolites no. 41, 42, 43 would fit into the zinnwaldite-type sheet more easily than those of some micas in the middle of the join. The approximately constant number of trivalent cations, which had been noted by Foster (1960b), shifts octahedral vacancies into large octahedral sites.

16	1	22	17	41	43	42	45
1.08	1.99	1.78	1.80	1.55	1.57	1.70	1.89
0.11	0.10	c	c	0.12	0.15	0.11	0.10
+	+	c	c	0.04	0.05	0.06	—
0.09	0.05	0.17	0.19	0.07	0.07	0.03	0.14
0.08	0.08	0.04	0.11	0.02	0.03	0.02	+
0.64	−0.22	0.01	−0.10	0.20	0.13	0.08	−0.13
1.83	2.20	2.12	2.54	3.22	2.95	3.15	3.92
1.37	1.24	1.11	0.52	0.01	+	+	+
0.03	+	0.06	+	0.13	0.11	0.12	0.07
0.07	0.14	0.06	0.08	0.10	0.06	0.02	—
2.04	1.98	2.10	2.12	2.34	2.56	2.48	1.91
0.22	0.12	0.16	0.27	0.04	0.02	0.01	0.01
—	—	—	—	—	+	+	—
1.69	1.35	1.40	0.98	0.84	1.04	0.96	—
6.29	6.64	6.57	7.01	7.16	6.96	7.04	8.00
0.02	0.01	0.03	0.01	b	b	b	0.05 (oct)
20.00	20.00	20.00	20.00	20.00	20.00	20.00	20.00
2.75	2.41	3.40	3.32	3.03	3.16	3.07	3.28
1.25	1.59	0.60	0.68	0.97	0.84	0.93	0.72
—	—	—	—	—	—	—	—
0.26	0.86	0.60	—	0.50	0.45	0.85	0.04
5.56	5.68	5.61	5.53	5.84	5.70	5.78	5.96
11.55	11.26	11.36	10.91	10.84	11.03	10.90	10.02
0.718	0.753	0.784	0.888	0.977	0.989	0.996	1.000
0.560	0.604	0.645	0.799	0.956	0.977	0.992	1.000
0.980	1.000	0.951	1.000	0.458	0.353	0.143	0.000
0.008	0.000	0.014	0.000	0.027	0.021	0.024	0.017
0.077	−0.018	0.025	−0.027	−0.144	−0.065	−0.114	−0.327

It had been known that an increase of lithium is accompanied by a decrease of iron (Foster, 1960b; Sitnin and Razina, 1963; Povilaitis and Organova, 1963). Foster's plot is indicative of replacement, but does not give a clear ratio. This is due to the interference of octahedral vacancies. In Fig. 7, micas with $\Sigma \text{oct} \geqq 5.5$ are marked with heavy solid circles and outline the replacement better than do micas with more vacancies. Iron-rich compositions approach the 4:4 ratio, while the 6:3 ratio holds for lepidolites no. 41, 42, 43 and is approached by a few other micas.

A correlation between lithium and fluorine had been mentioned (Foster, 1960b; Sitnin and Razina, 1963). The fact that the ratio F:Li is mostly larger than unity was noted by Povilaitis and Organova (1963) and follows also from Fig. 8. This indicates a crystallochemical association between lithium and fluorine.

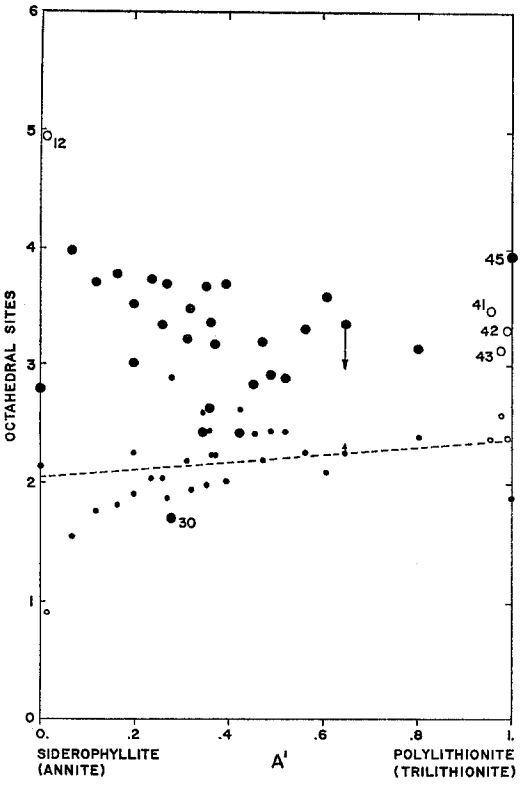

Fig. 6

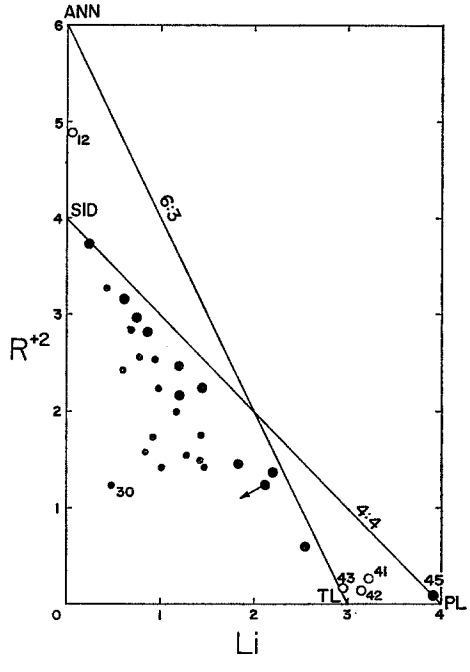

Fig. 7

Fig. 6. Small octahedral cations (Al, Fe^{+3}, Cr^{+3}; small circles) and large octahedral cations (Li, Fe^{+2}, Mn^{+2}, Mg; large circles) of lithium-iron micas plotted against A'. The broken line is a regression line for the number of small cations in ordered micas (solid circles). Other symbols as in Figs. 4, 5

Fig. 7. Relation between atomic quantities of lithium and bivalent octahedral cations (R^{+2}) in lithium-iron micas. Large circles mark micas with $\Sigma oct \geqq 5.5$. Lines representing 4:4 replacement along the siderophyllite-polylithionite (SID-PL) join and the 6:3 replacement along the annite-trilithionite (ANN-TL) join are shown for comparison. Symbols as in Figs. 4, 5

A plot of atomic quantities of R^{+4} against lithium is shown in Fig. 9. Several points lie near the annite-trilithionite join, but the spread of points bears resemblance to the siderophyllite-polylithionite join. Surprisingly, lepidolites no. 41, 42, 43 plot close to the siderophyllite-polylithionite join. The correlation between R^{+4} and Li in Fig. 9 is better than in Foster's (1960b) plot.

2.4.1. Vacancies

Almost all "trioctahedral" micas contain octahedral and interlayer vacancies. If fully occupied micas can be synthesized, why are vacancies so ubiquitous in natural micas? If they are a function of temperature, pressure, phases in equilibrium with the mica, or fugacities of volatiles[8], they may provide additional information on the growth conditions.

8 This was confirmed by a study of synthetic lithium-iron micas (to be published).

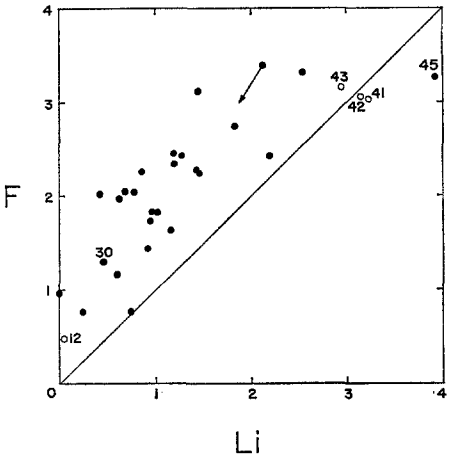

Fig. 8

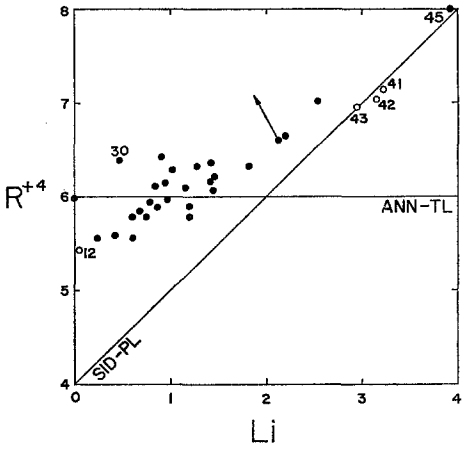

Fig. 9

Fig. 8. Relation between atomic quantities of lithium and fluorine in lithium-iron micas. A line corresponding to 1:1 ratio is shown for comparison. Symbols as in Figs. 4, 5

Fig. 9. Relation between atomic quantities of lithium and R^{+4} in lithium-iron micas. Symbols as in Figs. 4, 5; abbreviations as in Fig. 7

In examining octahedral vacancies we shall assume no interlayer vacancies (filled with oxonium) and a zero effect of interlayer bivalent cations and oxygen in (OH, F) sites on the charge relations within the mica. This is justified as the number of vacancies is subject to a larger uncertainty inherent in the method of calculation of crystallochemical formulas (*cf.* columns (2) and (6) in Table 2; see Fig. 11). Then the octahedral vacancies can form by (i) tetrahedral substitution of R^{+4} for R^{+3} and (ii) substitutions within the octahedral sheet itself at constant octahedral charges (Roman numerals denote coordination, solid circles represent vacancies):

Tetrahedral

$$\tfrac{1}{3}\,R^{+3}_{VI} + R^{+3}_{IV} \rightarrow \tfrac{1}{3}\bullet_{VI} + R^{+4}_{IV}$$
$$\tfrac{1}{2}\,R^{+2}_{VI} + R^{+3}_{IV} \rightarrow \tfrac{1}{2}\bullet_{VI} + R^{+4}_{IV}$$
$$R^{+1}_{VI} + R^{+3}_{IV} \rightarrow \bullet_{VI} + R^{+4}_{IV}$$

Octahedral

$$1\tfrac{1}{2}\,R^{+2}_{VI} \rightarrow \tfrac{1}{2}\bullet_{VI} + R^{+3}_{VI}$$
$$3\,R^{+1}_{VI} \rightarrow 2\bullet_{VI} + R^{+3}_{VI}$$
$$2\,R^{+1}_{VI} \rightarrow \bullet_{VI} + R^{+2}_{VI}$$

Vacancies created by octahedral and tetrahedral substitutions, respectively, were calculated (see Appendix) for all micas of Tables 3 and 4 and are plotted in Fig. 12. The ratio of OCT to TETR in Fig. 12 is mostly close to two, irrespective of the total number of vacancies. At this point it is not possible to interpret this result.

Fig. 10 shows the relation between ratios a and b (see Appendix) and occupancy of an octahedral sheet that contains two trivalent cations, as was suggested by Fig. 6. The occupancies read off the nomograph compare poorly with those listed in Table 4. The octahedral sheets of a few micas must accommodate more than two trivalent cations, thus distorting or precluding octahedral ordering.

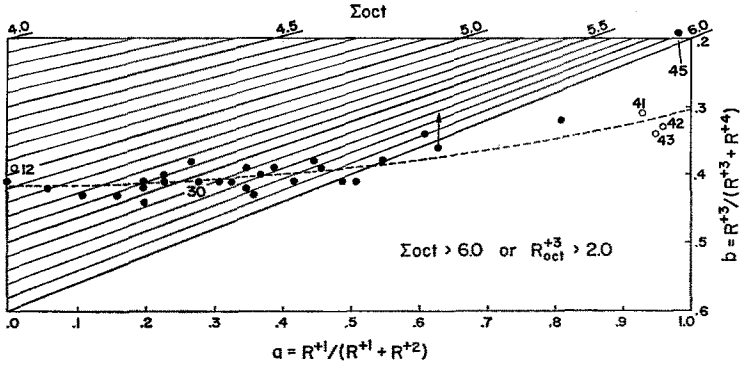

Fig. 10. Octahedral occupancy (Σoct) as a function of ratios a and b; two octahedral R^{+3} are assumed to be present. The occupancies of natural lithium-iron micas compare poorly with those found from their a and b ratios. There is, however, a relation between a and b; the dashed line is a corresponding regression curve (sample 45 not considered). R^{+1}, R^{+2}, R^{+3}, R^{+4} are octahedral and tetrahedral cations. Other symbols as in Figs. 4, 5

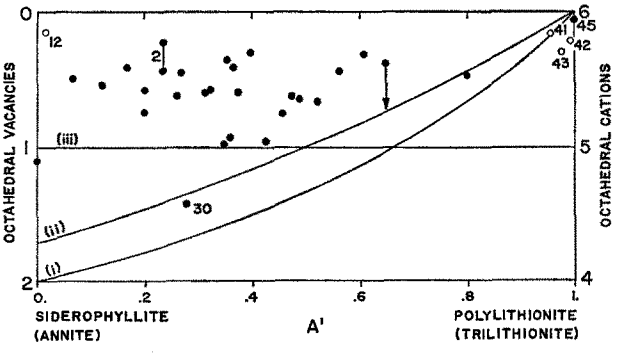

Fig. 11

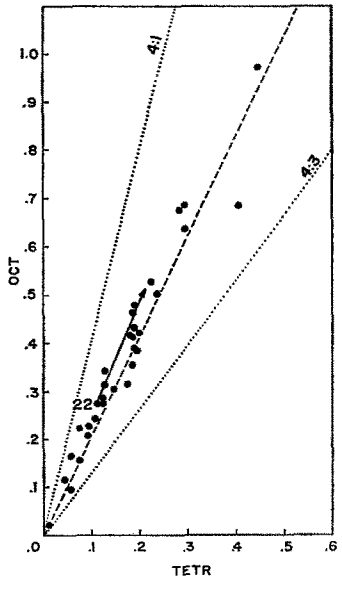

Fig. 12

Fig. 11. A plot of octahedral vacancies/cations against A′. The range given for sample no. 2 shows the uncertainty due to different methods of calculation of crystallochemical formula (Table 2). Lines (i), (ii), (iii) give octahedral vacancies generated by tetrahedral substitutions using different assumptions (see 2.4.1). Symbols as in Figs. 4, 5

Fig. 12. A plot of octahedral vacancies created by octahedral substitutions (OCT) against those created by tetrahedral substitutions (TETR) in lithium-iron micas (all marked with solid circles). The broken line is a regression line for the data; the dotted lines show hypothetical alternatives (see Appendix). Symbols as in Fig. 5

The maximum numbers of vacancies created by tetrahedral substitutions were calculated for ideal compositions along the siderophyllite-polylithionite join (curves (i) and (ii) in Fig. 11) and along the annite-trilithionite join (curve (iii) in Fig. 11). In case (i), the presence of two trivalent octahedral cations was assumed in deficient sheets; in cases (ii) and (iii), the ratios $Li:Fe^{+2}:Al$ of deficient sheets were identical with those of fully occupied ones. Even though octahedral substitutions create about twice as many vacancies as do the tetrahedral ones (Fig. 12), the total number of vacancies in most of the micas is less than the maximum permitted by tetrahedral substitutions alone (Fig. 11).

Octahedral compositions with vacancies due to tetrahedral substitutions according to (ii) and (iii) of Fig. 11 plot in Fig. 5 in the same place as their fully occupied counterparts. Case (i) increases R^{+3}_{exc} in relation to Σoct; octahedral compositions corresponding to curve (i) of Fig. 11 plot on a line combining point A with polylithionite in Fig. 5. Compositions of octahedral sheets with vacancies formed by octahedral substitutions R^{+1}, $R^{+2} \rightarrow R^{+3}$ also plot above their starting join.

2.4.2. Contaminated Micas

If the charge for analysis contains quartz, topaz, or feldspar in addition to mica, and if the analysis is treated as that of a mica, the resulting formula is distorted. Ten weight percent silica were added to the analysis of sample no. 22, and a crystallochemical formula was calculated. The formulas of pure and contaminated mica compare as shown alongside (symbols as in Table 4).

	22 pure	22 + 10 wt.% SiO_2
K	1.78	1.57
Rb	c	c
Cs	c	c
Na	0.17	0.15
Ca	0.04	0.03
H_3O	0.01	0.25
Li	2.12	1.87
Fe^{+2}	1.11	0.98
Mg	0.06	0.06
Mn^{+2}	0.06	0.06
Al	2.10	2.17
Fe^{+3}	0.16	0.14
Al	1.40	0.92
Si	6.57	7.06
Ti	0.03	0.02
O	20.00	20.00
F	3.40	3.00
OH	0.60	0.86
O	—	0.14
v	0.60	—
Σ oct	5.61	5.28
Σ (+) oct	11.36	11.00
A	0.784	0.782
A′	0.645	0.643
B	0.951	0.945
C	0.014	0.016
Q	0.025	0.083

The composition of contaminated no. 22 is shown in Figs. 5—12 as the endpoint of a vector whose origin marks the composition of pure no. 22.

Values of R^{+3}_{exc} and Q of the contaminated mica increase due to an apparent overflow of R^{+3} from the tetrahedral sheet into octahedral, and the point representing the apparent octahedral composition is shifted towards the muscovite apex (Fig. 5). Plots involving R^{+4} (Figs. 9, 10) are sensitive to contamination. The change of total small and large octahedral cations with contamination is shown in Fig. 6. The decrease of coefficients for Li, R^{+2}, and F, concurrent with the increase of R^{+4}, causes small shifts in Figs. 7 and 8. The number of vacancies is subject to a major change as follows from Figs. 11 and 12.

The behavior of a mica contaminated with feldspar and topaz would be similar to that of no. 22 contaminated with silica. The shift in Fig. 9 may be small; if the ratio $\frac{R^{+3}}{R^{+3}+R^{+4}}$ of the admixture approaches that of the mica, the mica will not deviate from the trend in Fig. 10.

Contamination may be suspected if the mica deviates from the trend in *more diagrams*. As transitional micas might exist, one should consult plots of physical parameters against composition[10]. *Physical properties of contaminated micas must plot in line with those of pure micas*. Deviations from the trend in both composition plots and plots of physical parameters indicate a mica of unusual composition. So, contamination of mica no. 30 is to be suspected from its behavior in composition plots[11].

3. Nomenclature of Lithium-Iron Micas

Chemical compositions and crystallographic data indicate the existence of a solid-solution series between *siderophyllite* and *polylithionite*. A simplified formula for the series is $K_2Fe_x^{+2}Li_{4-x}(Al, Fe^{+3})_2Al_xSi_{8-x}O_{20}(OH, F)_4$; x is four in siderophyllite and zero in polylithionite. I propose that *zinnwaldite* be given a range formula, with $1 \leqq x \leqq 3$. Micas with $x < 1$ should be termed *ferroan polylithionite*, with $x > 3$, *lithian siderophyllite*. Use of the name "*cryophyllite*" (Table 1) is discouraged, for it is covered by ferroan polylithionite, ferroan trilithionite (generally: ferroan lepidolite), or zinnwaldite. More precise variety names *lithian siderophyllite* and *lithian annite* should be preferred to "*Li-biotite*". "*Protolithionite*", $K_2LiFe_4^{+2}AlAl_2Si_6O_{20}(OH)_4$ (Winchell, 1942), does not lie on the siderophyllite-polylithionite join. The name "*protolithionite*" should be used for *compositions corresponding to its original formula* if such compositions exist. The name "*lithium muscovite*" should be superseded by *trilithionite* as it is not a lithium analog of muscovite and invites confusion with *lithian muscovite*, a variety name for a lithium-containing muscovite. The formula of trilithionite is $K_2Li_3Al_3Al_2Si_6O_{20}(OH, F)_4$.

The formulas given here and in Table 1 represent idealized compositions. Vacancies have not been included inasmuch as their behavior is incompletely understood. Besides, they represent an additional variable: For example, a realistic formula for siderophyllite end member can be written as

$$K_2Fe_{3-4}^{+2}(Al, Fe^{+3})_2Al_{2-4}Si_{6-4}O_{20}(OH, F)_4.$$

When applied to natural compositions, the above names may require a modifying adjective.

Acknowledgements. I am indebted to Dr. H. P. Eugster for his guidance and advice. He and Dr. G. W. Fisher read drafts of the manuscript and suggested many improvements. Valuable oral or written discussions were held with Dr. P. Černý, Dr. M. Fleischer, Dr. M. D. Foster, Dr. C. Frondel, Dr. M. Ross, Dr. M. Štemprok, and Dr. Z. Šulcek.

Most of this paper was a part of a Ph. D. Thesis (Rieder, 1968b). The research was aided by NSF Grant GP-5064, H. P. Eugster principal investigator; by stipends and fellowships from The Johns Hopkins University; and by the Ústřední ústav geologický. All support is gratefully acknowledged.

10 The A, A′, B, and C ratios are not affected by contamination with common greisen minerals, and it is legitimate to use them as abscissae in such plots.

11 More discussion of sample no. 30 will appear in Part B.

Appendix. Calculation of Octahedral Vacancies Created by Octahedral and Tetrahedral Substitutions, Respectively

If we want to compare numbers of sites vacated by individual kinds of substitutions, we have to know the hypothetical "initial" fully occupied formula. In order to calculate it, we need the "present" cation-deficient formula and additional restrictions. Two restrictions follow from a comparison of the plot of $\frac{R^{+3}}{R^{+3}+R^{+4}}$ vs. $\frac{R^{+1}}{R^{+1}+R^{+2}}$ (Fig. 10) with plots of octahedral vacancies against $\frac{LR}{LR+\text{"Fe"}}$ (Fig. 11; $\frac{R^{+1}}{R^{+1}+R^{+2}}$ is close to or identical with $\frac{LR}{LR+\text{"Fe"}}$ as $LR = R^{+1}$ for most of the join; as Mg approaches zero, "Fe" approaches R^{+2}) and against $\frac{R^{+3}}{R^{+3}+R^{+4}}$ (not shown). The small vertical scatter in Fig. 10 constrasts to the large scatter in Fig. 11. It follows that $\frac{R^{+3}}{R^{+3}+R^{+4}}$ is almost constant in micas with different numbers of vacancies. The same can be claimed of the $\frac{R^{+1}}{R^{+1}+R^{+2}}$ ratio. Both observations can be generalized into assumptions that ratios $\frac{R^{+1}}{R^{+1}+R^{+2}}$ and $\frac{R^{+3}}{R^{+3}+R^{+4}}$ of the cation-deficient formulas are identical with those of the fully occupied ones. A third restriction is an arbitrary assumption that the sum of octahedral and tetrahedral positive charges is independent of the number of vacancies.

Symbols:

r	coefficients of octahedral and tetrahedral cations in cation-deficient formula
R	coefficients of octahedral and tetrahedral cations in fully occupied formula
vac	octahedral vacancy
S	sum of positive octahedral and tetrahedral charges
oct	created octahedrally; octahedral (subscript)
tetr	created tetrahedrally (subscript)
1, 2, 3, 4	valence of cations; valence of cations being replaced by a vacancy (subscript)
Σoct	sum of octahedral cations

Assumptions: (i) The ratio of univalent to bivalent cations is independent of the number of octahedral vacancies

$$\frac{r_1}{r_1+r_2} = \frac{R_1}{R_1+R_2} = a.$$

(ii) The ratio of trivalent to quadrivalent cations is independent of the number of octahedral vacancies

$$\frac{r_3}{r_3+r_4} = \frac{R_3}{R_3+R_4} = b.$$

(iii) The total of positive octahedral and tetrahedral charges is independent of the number of octahedral vacancies

$$r_1+2r_2+3r_3+4r_4 = R_1+2R_2+3R_3+4R_4 = S.$$

(iv) The "initial" formula is fully occupied

$$R_1+R_2+R_3+R_4 = 14.$$

By solving we obtain

$$R_{3\text{oct}} = R_3 + R_4 - 8 = \frac{S - 44 + 6a + 8b}{2 + a - b}.$$

Due to (i), octahedrally created vacancies form by substitution of $r_{3\text{oct}}$ for R_1 and R_2 only. Due to (ii), tetrahedral substitutions create vacancies only at the expense of R_1 and R_2.

The following sets of equations yield the numbers of vacancies created by the respective processes:

octahedral

$$3(r_{3\text{oct}} - R_{3\text{oct}}) = \text{vac}_1' + 2\,\text{vac}_2'$$

$$\frac{\text{vac}_1'}{\text{vac}_1' + \text{vac}_2'} = a$$

$$\text{vac}_{\text{oct}} = \text{vac}_1' + \text{vac}_2' - (r_{3\text{oct}} - R_{3\text{oct}})$$

$$\downarrow$$

$$\text{vac}_{\text{oct}} = \frac{1+a}{2-a}(r_{3\text{oct}} - R_{3\text{oct}})$$

tetrahedral

$$(1-b)(r_{3\text{oct}} - R_{3\text{oct}}) = \text{vac}_1'' + 2\,\text{vac}_2''$$

$$\frac{\text{vac}_1''}{\text{vac}_1'' + \text{vac}_2''} = a$$

$$\text{vac}_{\text{tetr}} = \text{vac}_1'' + \text{vac}_2''$$

$$\downarrow$$

$$\text{vac}_{\text{tetr}} = \frac{1-b}{2-a}(r_{3\text{oct}} - R_{3\text{oct}})$$

Values of vac_{oct} and vac_{tetr} can be calculated from a, b, and Σoct as

$$\text{vac}_{\text{oct}} = (6 - \Sigma\text{oct})\frac{1+a}{2+a-b}$$

$$\text{vac}_{\text{tetr}} = (6 - \Sigma\text{oct})\frac{1-b}{2+a-b}.$$

The ratio $\text{vac}_{\text{oct}}/\text{vac}_{\text{tetr}} = \frac{1+a}{1-b}$ is arithmetically independent of the total number of vacancies. It can be shown that assumptions (i) to (iv) do not permit vacancies to form by either octahedral or tetrahedral substitutions alone. $\text{vac}_{\text{oct}}/\text{vac}_{\text{tetr}}$, however, can vary as is illustrated by two pairs of fully occupied and cation-deficient formulas:

Formula				Σ oct	vac_{oct}	vac_{tetr}	$\frac{\text{vac}_{\text{oct}}}{\text{vac}_{\text{tetr}}}$	a	b	S
K_2	$Li_{1.4}Fe^{+2}_{1.4}Al_{3.2}$	$Al_{3.8}Si_{4.2}$	$O_{20}(F, OH)_4$	6	0	0	—	$\frac{1}{2}$	$\frac{5}{8}$	42
K_2	$Li\ Fe^{+2}Al_{3\frac{5}{9}}$	$Al_{3\frac{2}{3}}Si_{4\frac{1}{3}}$	$O_{20}(F, OH)_4$	$5\frac{5}{9}$	$\frac{16}{45}$	$\frac{4}{45}$	4	$\frac{1}{2}$	$\frac{5}{8}$	42
K_2	$Li_{1.2}Fe^{+2}_{4.8}$	$Al_{0.8}Si_{7.2}$	$O_{20}(F, OH)_4$	6	0	0	—	$\frac{1}{5}$	$\frac{1}{10}$	42
K_2	$Li\ Fe^{+2}_4Al_{1\frac{6}{13}}$	$Al_{1\frac{5}{13}}Si_{7\frac{8}{13}}$	$O_{20}(F, OH)_4$	$5\frac{6}{13}$	$\frac{4}{13}$	$\frac{3}{13}$	$1\frac{1}{3}$	$\frac{1}{5}$	$\frac{1}{10}$	42

References

Bokii, G. B., Arkhipenko, D. K.: Ob oksonii v vermikulite. Zh. Strukt. Khim. **3**, 697—702 (1962).

Brown, G., Norrish, K.: Hydrous micas. Mineral. Mag. **29**, 929—932 (1952).

Cissarz, A.: Übergangslagerstätten innerhalb der intrusivmagmatischen Abfolge. Teil I. Zinn-Wolfram- und Molybdänformationen. Neues Jahrb. Mineral., Geol., Paläontol., Beilage-Bd. **56A**, 99—274 (1927).

Eugster, H. P., Munoz, J.: Ammonium micas: possible sources of atmospheric ammonia and nitrogen. Science **151**, 683—686 (1966).

Foster, M. D.: Interpretation of the composition of trioctahedral micas. U.S. Geol. Surv. Profess. Papers **354**-B, 11—48 (1960a).

— Interpretation of the composition of lithium micas. U.S. Geol. Surv. Profess. Papers **354**-E, 115—146 (1960b).

— Wones, D. R., Eugster, H. P.: The atomic ratios of natural ferruginous biotites with reference to 'The stability relations of the ferruginous biotite, annite' (a discussion). J. Petrol. **4**, 302—306 (1963).

Franzini, M.: The A and B mica layers and the crystal structure of sheet silicates. Contr. Mineral. and Petrol. **21**, 203—224 (1969).

Gottesmann, B.: Über einige Lithium-Glimmer aus Zinnwald und Altenberg in Sachsen. Geologie **11**, 1164—1176 (1962).

Grim, R. E., Bradley, W. F., Brown, G.: The mica clay minerals. Chapter V in: X-ray identification and crystal structures of clay minerals (ed. G. W. Brindley). London: Mineralogical Society 1951.

Hendricks, S. B., Ross, C. S.: Chemical composition and genesis of glauconite and celadonite. Am. Mineralogist **26**, 683—708 (1941).

Kovalenko, N. I., Kashaev, A. A., Znamenskii, E. B., Zhuravleva, R. M.: Otnositel'no vkhozhdeniya titana v slyudy (eksperimental'nye issledovaniya). Geokhimiya No. 11, 1348—1357 (1968).

Mikheev, V. I.: Vliyanie izomorfnogo zameshcheniya v slyudakh na kharakter debaegramm. Mineralog. Sb. L'vovsk. Geol. Obshchestva pri L'vovsk. Gos. Univ. 8, 261—280 (1954).

Munoz, J. L.: Physical properties of synthetic lepidolites. Am. Mineralogist **53**, 1490—1512 (1968).

Němec, D.: Glimmer der regionalmetamorphen Skarne Westmährens. Tschermaks Mineral. Petrog. Mitt. **13**, 55—84 (1969).

Nockolds, S. R., Richey, J. E.: Replacement veins in the Mourne Mountains granites, N. Ireland. Am. J. Sci. **237**, 27—47 (1939).

Pavlishin, V. I.: O kristallakh litievo-zhelezistykh slyud p'ezokvartsevykh pegmatitov. Mineralog. Sb. L'vovsk. Gos. Univ. im. I. Franko **19**, 85—88 (1965).

Povilaitis, M. M., Organova, N. I.: K voprosu o sostave i svoistvakh slyud. Tr. Mineralog. Muzeya Akad. Nauk SSSR **14**, 140—165 (1963).

Rankama, K., Sahama, T. G.: Geochemistry. Chicago: Chicago University Press 1950.

Rieder, M.: Zinnwaldite: octahedral ordering in lithium-iron micas. Science **160**, 1338—1340 (1968a).

— A study of natural and synthetic lithium-iron micas. Baltimore: Ph. D. Thesis, Johns Hopkins University 1968b.

Ross, M., Evans, H. T., Jr.: Studies of the torbernite minerals (III): role of the interlayer oxonium, potassium, and ammonium ions, and water molecules. Am. Mineralogist **50**, 1—12 (1965).

Sclar, C. B., Carrison, L. C., Schwartz, C. M.: High-pressure synthesis and stability of a new hydronium-bearing layer silicate in the system MgO-SiO_2-H_2O. Trans. Am. Geophys. Union **46**, 184 only (1965).

Serdyuchenko, D. P.: O kristallokhimicheskoi roli titana v slyudakh. Dokl. Akad. Nauk SSSR **59**, 739—742 (1948).

Sitnin, A. A., Razina, I. S.: O khimicheskom sostave litievykh slyud iz metasomaticheski izmenennykh granitov. Geokhimiya No. 7, 695—699 (1963).

Štemprok, M.: Remarks on the paragenetic position and chemical composition of zinnwaldite from Cínovec [Czech]. Věstn. Ústředního Ústavu Geol. **36**, 303—305 (1961).

— Genetic features of the deposits of tin, tungsten and molybdenum formation. In: Problems of postmagmatic ore deposition, vol. II, p. 472—481. Prague: Publishing House of the Czechoslovak Academy of Sciences 1965.

— Genetische Probleme der Zinn-Wolfram-Vererzung im Erzgebirge. Mineralium Deposita **2**, 102—118 (1967).

Stern, W. B.: Zur Mineralchemie von Glimmern aus Tessiner Pegmatiten. Schweiz. Mineral. Petrog. Mitt. **46**, 137—188 (1966).

Stevens, R. E.: New analyses of lepidolites and their interpretation. Am. Mineralogist **23**, 607—628 (1938).
Tröger, W. E.: Über Protolithionit und Zinnwaldit. Ein Beitrag zur Kenntnis von Chemismus und Optik der Lithiumglimmer. Beitr. Mineral. Petrog. **8**, 418—431 (1962).
White, J. L., Burns, A. F.: Infrared spectra of hydronium ion in micaceous minerals. Science **141**, 800—801 (1963).
Winchell, A. N.: Further studies of the lepidolite system. Am. Mineralogist **27**, 114—130 (1942).
Yakovleva, M. E., Razmanova, Z. P., Smirnova, M. A.: Lepidolit s malym uglom opticheskikh osei. Tr. Mineralog. Muzeya Akad. Nauk SSSR **16**, 287—292 (1965).

Milan Rieder
Ústav geologických věd University Karlovy
Albertov 6, Praha 2
Československo